JOURNAL OF CATALYSIS 87, 210–225 (1984)

Cleavage of Benzylaryl Ethers in the Presence of Zinc Halides

TIM J. FREDERICK[1] AND ALEXIS T. BELL

Materials and Molecular Research Division, Lawrence Berkeley Laboratory, and Department of Chemical Engineering, University of California, Berkeley, California 94720

Received March 30, 1983

Ether groups constitute one of the primary linkages between aromatic centers present in coal. During the liquefaction of coal under the influence of zinc halides, it is believed that these linkages are cleaved. The details of this process have been studied in the present investigation using benzylphenyl ether (BPE), benzyl-*p*-tolyl ether (BTE), and benzyl-1-naphthyl ether (BNE) to represent the ether structures present in coal. $ZnCl_2$ and $ZnBr_2$ were used as catalysts. $ZnCl_2$ was found to be catalytically inactive. However, in the presence of HCl it forms a stable adduct which is highly active. $HBr/ZnBr_2$ behaves in a manner analogous to $HCl/ZnCl_2$ but is tenfold more active. All three ethers react in a similar fashion. In each case cleavage occurs at the oxygen–methylene bond and is accompanied by a small degree of ether rearrangement to form the corresponding hydroxydiarylmethane. The reaction kinetics for BPE, BTE, and BNE can be described in terms of a carbocation mechanism. Rate coefficients for each of the elementary steps have been determined by simulation of the experimentally observed product concentration versus time profiles.

INTRODUCTION

Ether groups account for a large fraction of the oxygen present in coal and are one of the primary linkages between aromatic centers (*1–5*). During the conversion of coal to liquid products, these linkages are cleaved. It is well known that zinc halides are effective catalysts for the liquefaction of coal and it has been suggested that this may be due, in part, to their ability to promote the cleavage of aromatic ethers (*6–9*). In a recent study by Mobley and Bell (*10*), it was demonstrated that while diaryl ethers are not reactive, benzylaryl and dibenzyl ethers readily react in the presence of $ZnCl_2$. Complete elimination of oxygen to form water was observed with dibenzyl ethers, but oxygen bonded directly to an aryl group was converted to a hydroxyl group.

The catalytically active form of metal halide catalysts involved in the cleavage of aromatic ethers is not well defined. Anhydrous Lewis acids, such as $AlCl_3$ (*11*), $AlBr_3$ (*12*), and BBr_3 (*13*), are known to cleave aromatic ethers. Anhydrous $ZnCl_2$ might be expected to behave in a similar fashion, since it is known to complex strongly with many ethers (*14*). Hydrated Lewis acids, including $ZnCl_2$ (*15*), are strong Brønsted acids and could be expected to cleave ethers in a manner analogous to H_2SO_4 (*16*). Combinations of Lewis acids and hydrogen halides are also effective catalysts. Thus, for example, the combination of HCl with metal halides promotes the reaction of benzylaryl ethers more rapidly than HCl alone (*17–20*).

This paper reports on the results of an investigation aimed at determining the effects of zinc halide catalysts on the reactions of benzylaryl ethers. Three ethers were examined—benzylphenyl ether, benzyl-*p*-tolyl ether, and benzyl-1-naphthyl ether. $ZnCl_2$ and $ZnBr_2$ were used as catalysts, both with and without the addition of hydrogen halides. The primary purpose of this work was to establish the influence of ether structure and catalyst composition on the kinetics of ether cleavage and the distribution of products formed. A further pur-

[1] Present address: Stauffer Chemical Company, Richmond, Calif. 94804.

0021-9517/84 $3.00

pose was to identify the active form of the catalyst. Based on the data obtained, a mechanism was proposed for the catalyzed cleavage of benzylaryl ethers. The rate parameters associated with elementary steps in this mechanism were determined by modeling the observed reaction kinetics.

EXPERIMENTAL

Reactions were carried out in a 300-cm^3, 316-stainless-steel, stirred autoclave (Autoclave Engineers, Inc. Model ABP-300) fitted with a glass liner. A 30-cm^3, stainless-steel vessel was connected to the autoclave and the inlet gas manifold. This vessel was used to hold a solution of the reactant prior to its introduction into the autoclave. The temperature of the autoclave contents was monitored using a sheathed thermocouple and the pressure within the autoclave was measured using a Bourdon gauge. Liquid samples were taken through a $\frac{1}{8}$-in. sampling tube, which was cooled in an ice bath after emerging from the autoclave.

A run was initiated by sieving the dried catalyst and placing a weighed amount of the 100/170-mesh (147–88 μm) cut in a glass liner, together with 50 ml of solvent. If an additive such as water or benzyl chloride was to be used, the additive was introduced into the solvent using a microsyringe (Hamilton). The glass liner was quickly transferred to the autoclave, which was then sealed and flushed with nitrogen. The reactant was weighed and dissolved in 20 ml of solvent. This solution was transferred to the reactant-holding vessel, which was then flushed and pressurized with hydrogen. During the heatup of the autoclave, the reactant-holding vessel remained at room temperature. The autoclave was heated to 10 K above the desired reaction temperature and then the reactant solution was injected. The temperature dropped and leveled off at the desired reaction temperature within 15 s.

Analysis of the liquid sample was carried out by gas chromatography using a 3 mm × 3 m, stainless-steel column packed with 5% OV-101 on Chromosorb WHP. Product identification was made using a Finnigan 4023 GC–MS and verified by matching peak retention times with those of pure components.

Benzylphenyl ether (Frinton Labs), benzyl-1-naphthyl ether (Eastman Kodak), and benzyl-*p*-tolyl ether were used as reactants. The last was synthesized from *p*-cresol and benzyl bromide and purified by recrystallization from ethanol. *p*-Xylene (Mallinckrodt) and cyclohexane (MBC) were dried by refluxing under nitrogen in the presence of sodium. *p*-Xylene was the solvent in all runs except for a few runs in which mixtures of *p*-xylene and cyclohexane were used. The zinc halides, $ZnCl_2$ (MCB), $ZnBr_2$ (MCB), and ZnI_2 (Fischer Scientific), were dried for 88 h at 383 K in a vacuum oven immediately prior to use. All reagents were stored and prepared in a nitrogen-purged dry box. The surface area of the catalysts was measured using the three-point BET technique on a Quantasorb analyzer.

RESULTS

Preliminary experiments showed that in the presence of $ZnCl_2$, benzylphenyl ether (BPE) undergoes both rearrangement and cleavage. The reaction products in *p*-xylene solution are 2-hydroxydiphenylmethane, phenol, and benzylxylene. It was observed, though, that different batches of BPE gave widely different rates of reaction. Consideration of the possible causes suggested that an impurity in the BPE might be responsible for these variations. An experiment with purified BPE and dried $ZnCl_2$ gave very little conversion of BPE, supporting the idea that impurities were responsible for the enhanced conversion. The most probable impurity in BPE is an organic halide left over from the synthesis of the ether. Under the conditions of the present experiments, the chloride can react to release HCl, which is an active catalyst for the cleavage of ethers. The validity of this interpretation was confirmed by experiments in which measured amounts of ben-

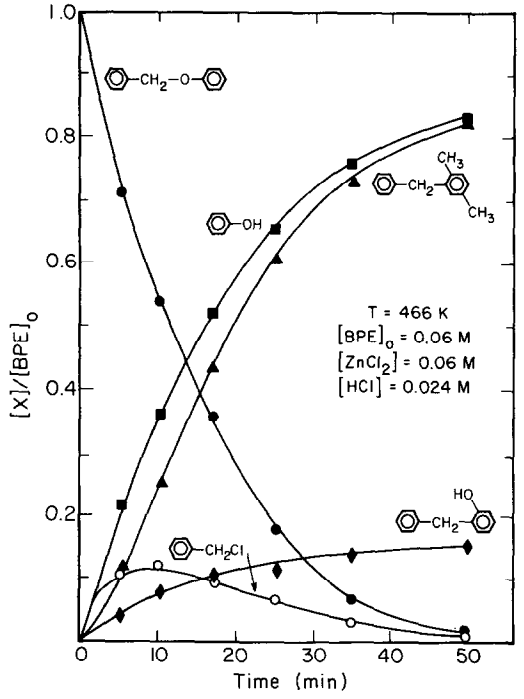

FIG. 1. Concentration versus time profiles observed for BPE.

zyl chloride were added to the *p*-xylene–catalyst mixture prior to heatup of the autoclave. It was observed that benzyl chloride rapidly reacted with the *p*-xylene to produce benzylxylene and HCl. When the BPE was then added to the solvent, it reacted much more rapidly than in the absence of HCl.

To determine whether the source of HCl had an effect on the reaction of BPE, experiments were carried out using 2-chloro-2-methylbutane instead of benzyl chloride. Both sources of HCl gave identical results indicating that the alkyl group does not play a role in the reaction and that HCl from different chloride sources has an identical effect. It was noted, though, that while the majority of the 2-chloro-2-methylbutane reacted with the solvent to form the alkylbenzene, a portion reacted to form pentene and HCl. Since the pentene escaped from the solution, it was difficult to establish accurately the amount of HCl released. As a consequence, all subsequent work was carried out using benzyl chloride as the source of HCl. The amount of HCl released was determined by the amount of benzylxylene formed.

Figure 1 shows the variation in product and reactant concentrations with time, during the reaction of BPE in the presence of $ZnCl_2$ and HCl. Two reactions paths can be discerned. The first is cleavage of BPE to yield phenol and benzyl chloride. The benzyl chloride then reacts with the *p*-xylene to form benzylxylene. The second path is rearrangement of BPE to form *o*-benzylphenol. Rearrangement accounts for 15% of BPE reacted, while cleavage accounts for 85%. The split between these two pathways remains relatively constant during the reaction. Figure 2 presents a similar plot for the reaction of benzyl-*p*-tolyl ether (BTE). The same two reaction paths for BTE lead to the production of *p*-cresol, benzylxylene, and 2-benzyl-4-methylphenol. Benzyl chloride is again observed as an intermediate product. Figure 3

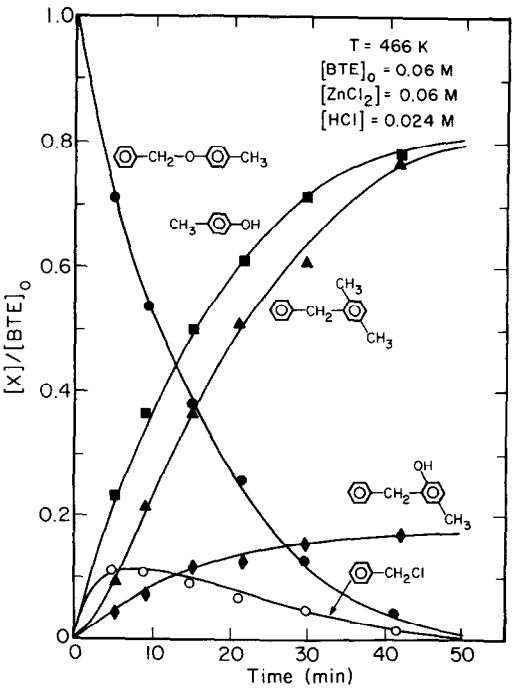

FIG. 2. Concentration versus time profiles observed for BTE.

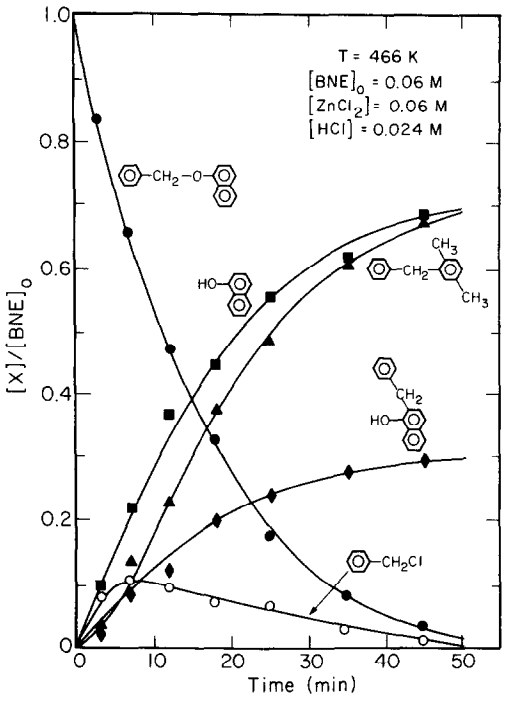

FIG. 3. Concentration versus time profiles observed for BNE.

shows the concentration versus time curves for the third ether, benzyl-1-naphthyl ether (BNE). Again, two reaction paths are found. Cleavage forms 1-naphthol and benzylxylene with the intermediate appearance of benzyl chloride. Rearrangement gives two isomers of benzyl-1-naphthol. The only difference compared to the reactions of BPE and BTE is that the rearrangement of BNE occurs to a greater degree.

As shown in Fig. 4, a plot of the logarithm of ether concentration versus time is a linear function. This indicates that the consumption of each of the three ethers follows first-order kinetics with respect to ether concentration. The slope of the line is the apparent, first-order rate coefficient, k_a.

The effect of HCl addition on k_a is shown in Fig. 5. It can be seen that the apparent rate coefficient increases with HCl in a nonlinear fashion. In the absence of HCl addition k_a is very small, approximately 2×10^{-5} s^{-1}. The solid points in Fig. 5 were obtained using a $ZnCl_2$ loading of 0.060 *M*. These points show the effect of increasing HCl concentration at a constant $ZnCl_2$ concentration. The open point was obtained using a $ZnCl_2$ loading of 0.078 *M*. The data in Fig. 5 show quite clearly that k_a depends on the concentration of HCl, but not on the $ZnCl_2$ concentration or the HCl/$ZnCl_2$ ratio.

Values of k_a and the product yields are presented in Table 1, for the reactions of BPE, BTE, and BNE under various conditions. The product yields were obtained at 100% conversion of the ether. The relative yields of products are constant during a run if the yield of benzylxylene is considered as the sum of the concentrations of benzylxylene and benzyl chloride. The yields of phenol and benzylxylene are roughly equal in each run. The sum of the phenol and benzylphenol yields is close to one in each case. The only other product observed is a trace of toluene (<1%). Only the *ortho* isomers and benzylphenol and benzyl-*p*-cresol are observed, but two isomers of benzylnaphthol are found. The extent of rearrangement is similar for BPE and BTE, typ-

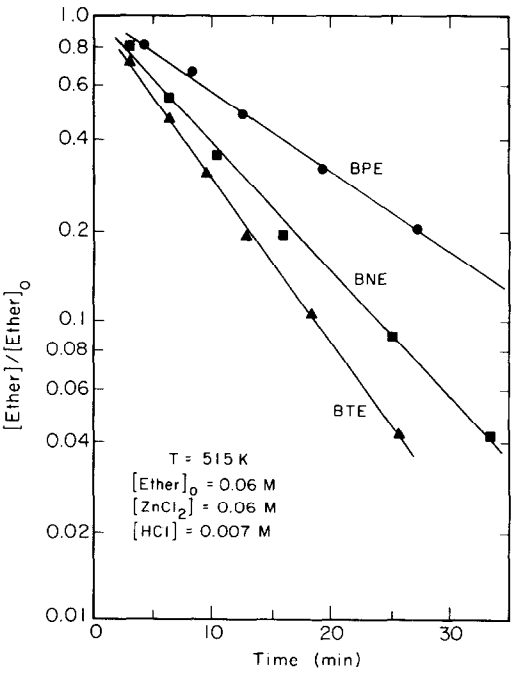

FIG. 4. Plot of log[ether]/[ether]$_0$ versus time.

TABLE 1

Product Yields and Rate Coefficients for the Reactions of BPE, BNE, and BTE[a]

Ether	T (K)	HCl concn (M)	Yield (%)			$k_a \times 10^{-3}$ (s^{-1})
			Phenol	Benzylxylene	Benzylphenol	
BPE	466	0.007	82	83	17	0.086
	466	0.024	85	85	15	1.1
	495	0.007	81	81	19	0.40
	503	0.007	85	80	16	0.72
	515	0.007	85	81	15	1,0
BNE	466	0.024	69	69	31	1.1
	495	0.007	67	67	31	0.58
	515	0.007	67	67	29	1.6
BTE	466	0.024	84	76	16	1.0
	495	0.007	81	75	19	0.86
	515	0.007	81	75	18	2.1

[a] All reactions were carried out in *p*-xylene using a 0.06 *M* loading of $ZnCl_2$ and an initial ether concentration of 0.06 *M*.

ically 15–20%. The extent of BNE rearrangement is noticeably higher, and is typically in the range of 30%.

Table 1 shows that the product distributions change very little with temperature.

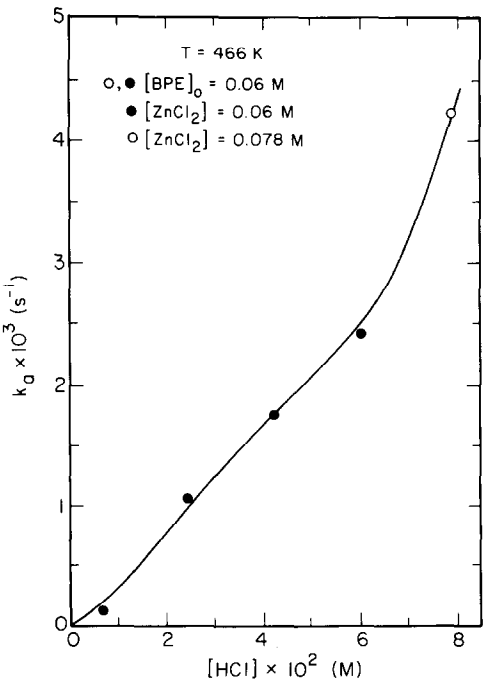

FIG. 5. Effect of HCl Concentration on k_a.

The magnitude of k_a increases with increasing temperature, as would be expected. The apparent rate coefficients for the three ethers are almost equal to 466 K, but above that temperature, the order of reactivity is BTE > BNE > BPE, as indicated in Fig. 4. The rate coefficients at different temperatures are not directly comparable because different levels of HCl were used.

The effects of several other variables are shown in Table 2. The apparent rate coefficient for BPE is unaffected by changing the ether loading. Water addition also has no effect on the reaction rate, but the rate is strongly affected by the solvent composition. Using 50% cyclohexane–50% *p*-xylene in place of 100% *p*-xylene results in a fourfold decrease in k_a from 2.8×10^{-4} to 10.8×10^{-4} s^{-1}, and the product yields shift slightly in favor of rearrangement. Hydrogen pressure does not affect the reaction rate or the product yields for any of the systems considered.

When an $HBr/ZnBr_2$ combination was used in place of $HCl/ZnCl_2$, the value of k_a increased tenfold, as shown in Table 2. It was also observed that the proportion of cleavage relative to rearrangement was greater in the bromide system than in the chloride system.

TABLE 2

Product Yields and Rate Coefficients for the Reactions of BPE at 466 K[a]

BPE concn (*M*)	Condition	Yield (%)			$k_a \times 10^{-3}$ (s^{-1})
		Phenol	Benzylxylene	Benzylphenol	
0.06	—	85	85	15	1.1
0.12	—	82	82	15	1.1
0.06	0.024 *M* H_2O	80	82	17	1.1
0.06	50% Cyclohexane 50% *p*-Xylene	81	79	20	0.28
0.06	HBr/ZnBr	92	93	06	9.4

[a] Unless otherwise noted, reactions were carried out in *p*-xylene using a $ZnCl_2$ loading of 0.06 *M* and an HCl loading of 0.02 *M*.

Experiments were also performed using $HCl/ZnBr_2$ and $HBr/ZnCl_2$ as the catalysts for the reaction of BPE. When the halide of the zinc differed from the halide of the hydrogen halide, the reaction no longer followed first-order kinetics. With $HCl/ZnBr_2$, the reaction at first followed a pattern similar to that observed for $HCl/ZnCl_2$. As shown in Fig. 6, the initial rate of ether disappearance is similar to that observed in the presence of $HCl/ZnCl_2$ reaction and benzyl chloride is formed as the intermediate. As the reaction proceeds, benzyl bromide appears and the rate of reaction increases. The reverse behavior occurs with $HBr/ZnCl_2$. In this case, the initial rate is comparable to that observed with $HBr/ZnBr_2$. After some time, benzyl chloride appears and the rate of reaction decreases. Table 3 shows the maximum yields of benzyl halide during these experiments. The maximum yield is the ratio of the maximum observed benzyl halide concentration to the initial ether concentration. At least 2% of the halide originally associated with the zinc appeared as benzyl halide in the mixed halide runs. It is apparent from these exper-

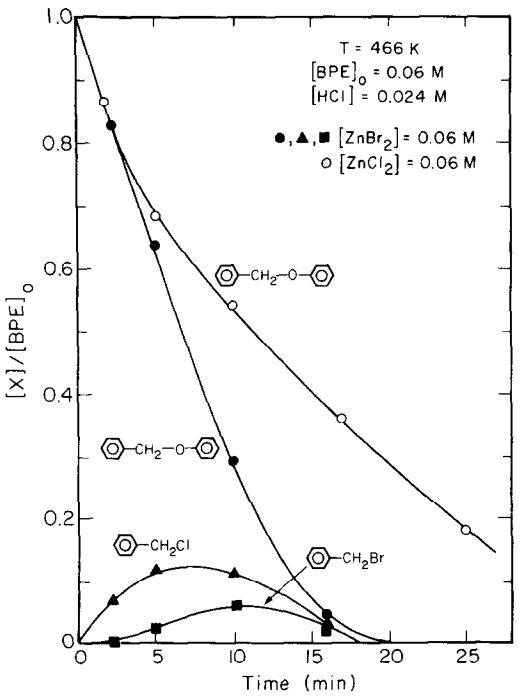

FIG. 6. Comparison of the concentration versus time plots for the reaction of BPE in the presence of HCl/$ZnCl_2$ and $HCl/ZnBr_2$.

TABLE 3

Maximum Yield of Benzyl Halide in the Reaction of BPE[a]

	Yield (%)			
Benzylchloride	12	11	4	—
Benzylbromide	—	4	11	16

[a] All reactions were carried out at 466 K in *p*-xylene using a $ZnCl_2$ loading of 0.06 *M*, an HCl loading of 0.024 *M*, and an initial concentration of BPE equal to 0.06 *M*.

TABLE 4

Apparent Rate Coefficients for Reactions of BPE in the Presence and Absence of $ZnCl_2$[a]

Catalyst	Apparent rate coefficient (s^{-1})		
	30-min heatup 0.024 *M* HCl	40-min heatup	
		0.024 *M* HCl	0.042 *M* HCl
HCl	1.2×10^{-3}	2.8×10^{-4}	5.8×10^{-4}
$HCl/ZnCl_2$[b]	1.1×10^{-3}	1.2×10^{-3}	1.8×10^{-3}

[a] All reactions were carried out at 466 K in *p*-xylene.
[b] $[ZnCl_2] = 0.06$ *M*.

iments that a significant amount of halide exchange occurs between the hydrogen halide and the zinc halide during the course of the reaction.

To determine the separate roles of HCl and $ZnCl_2$, several experiments were conducted in the absence of $ZnCl_2$. Table 4 compares the apparent rate coefficients for runs with and without $ZnCl_2$. In runs carried out without $ZnCl_2$, HCl was generated via the thermal reaction of benzyl chloride with the solvent. While the release of HCl is significantly slower in the absence of $ZnCl_2$, it was found that all of the benzyl chloride could be reacted within 30 min. This is 5 min longer than the time required to heat the autoclave to 476 K. Reaction with and without $ZnCl_2$ gave the same rate, following a 30-min heatup. If the autoclave was held at 476 K for an additional 10 min (40-min heatup), a different behavior was observed. The experiment with $HCl/ZnCl_2$ gave the same results as before, but the experiment conducted with HCl alone resulted in a threefold decrease in the initial reaction rate, as shown in Fig. 7. The rate decreased as the reaction proceeded, and the reaction no longer followed first-order kinetics. It is believed this behavior was due to a loss of HCl from the solution, especially during the heatup period.

The preceding experiments suggest that $ZnCl_2$ interacts with the free HCl and thereby eliminates the loss of HCl from solution. If this interpretation is correct, the reaction rate should depend on the amount of HCl available at the $ZnCl_2$ surface and,

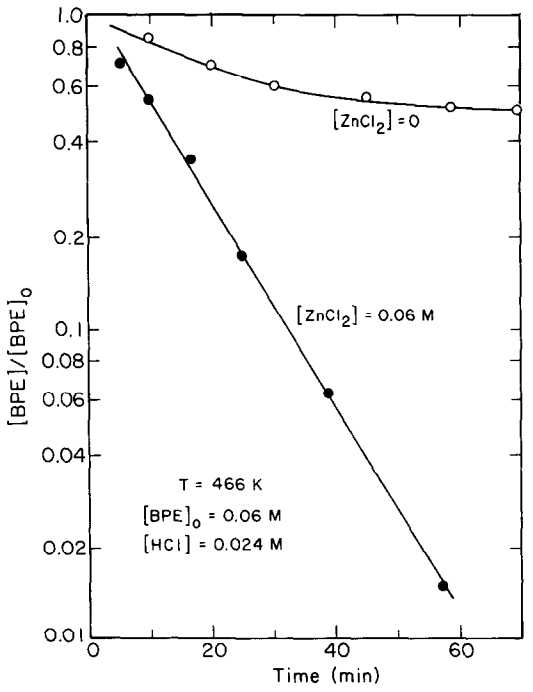

FIG. 7. Comparison of the rates of reaction of BPE in the presence of $HCl/ZnCl_2$ and HCl alone.

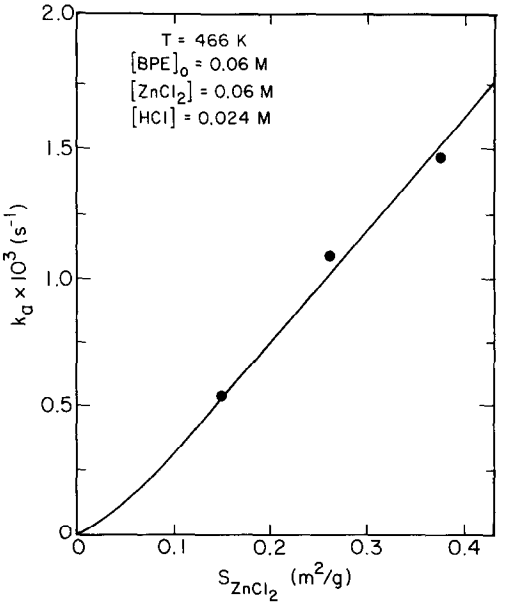

FIG. 8. Effect of $ZnCl_2$ surface area on k_a.

therefore, on the surface area of $ZnCl_2$. The effect of surface area on reaction rate was investigated by conducting experiments using $ZnCl_2$ particles exhibiting different surface areas. The apparent, first-order rate coefficients are plotted against the $ZnCl_2$ surface area in Fig. 8. An HCl concentration of 0.024 *M* was used in each run. It is apparent from Fig. 8 that k_a increases with the BET surface area of $ZnCl_2$, consistent with the proposed interpretation.

The reaction of benzyl chloride with xylene occurs during both the generation of HCl and the reaction of the ethers. The kinetics of this reaction were studied in a separate set of experiments, to determine the effects of temperature and HCl addition. In the presence of a large excess of *p*-xylene, it was found that the rate of the reaction

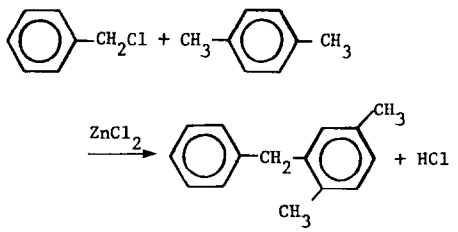

is first order in the concentration of benzyl chloride. A plot of the apparent, first-order rate coefficient is shown as a function of temperature in Fig. 9. The slope of the line gives an activation energy of 14.6 kcal/mole. The addition of HCl to the $ZnCl_2$ retards the reaction. Thus, starting with $ZnCl_2$ alone, the rate coefficient is 5×10^{-3} s^{-1} at 466 K. Addition of 1.0 mole HCl per mole $ZnCl_2$ before reaction of the benzyl chloride reduces the rate coefficient to 3.1×10^{-3} s^{-1}.

DISCUSSION

Reaction Mechanism

Under the conditions of the present investigation, $ZnCl_2$ exhibits relatively little activity for catalyzing either the cleavage or the rearrangement of BPE. HCl, on the other hand, readily promotes both reactions but is lost from solution in the absence of an imposed partial pressure of gaseous HCl. When HCl and $ZnCl_2$ are present together, the $ZnCl_2$ stabilizes the dissolved HCl, presumably through the formation of a complex. Since the rate of reaction increases with increasing surface area of the $ZnCl_2$ particles, it appears that catalysis occurs at the surface of the solid $ZnCl_2$ particles. Qualitatively similar behavior is observed using $HBr/ZnBr_2$, $HCl/ZnBr_2$, and $HBr/ZnCl_2$ as the catalysts.

The mechanism shown in Fig. 10 can be used to explain the reactions of benzylaryl ethers in the presence of $HCl/ZnCl_2$. The active catalyst is assumed to be an adduct of HCl and $ZnCl_2$. Since the structure of this complex is not known, it will be designated as $HCl \cdot ZnCl_2$ for the purpose of the present discussion. In the first step of the reaction sequence, it is assumed that an adduct is formed between the electron-rich oxygen atom of the ether and the proton associated with the complex. This reaction

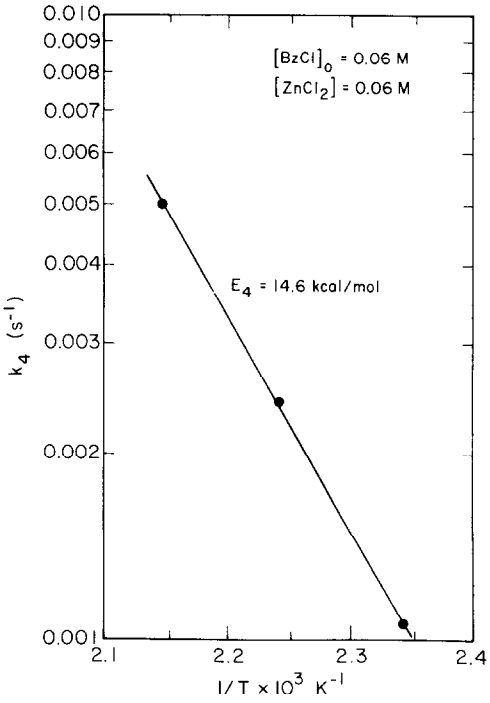

FIG. 9. Arrhenius plot for k_4.

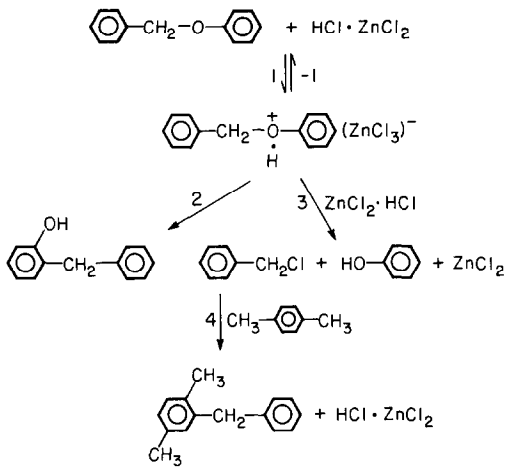

FIG. 10. Proposed mechanism for the reaction of BPE in the presence of HCl · $ZnCl_2$.

parallels the formation of tightly bound adducts known to occur between HCl and various ethers (*21, 22*). The protonated ether can react via two paths. Reaction 3 results in a rearrangement of BPE to *o*-benzylphenol. The appearance of only the *ortho* isomer is indicative of intramolecular rearrangement, a common reaction for aromatic ethers (*23*). The *para* isomer is not formed because the isomerization of hydroxydiphenylmethane is slow under the conditions used in the present study (*24*). The second reaction path for the protonated ether involves dissociation into phenol and benzyl chloride, reaction 2. These are the products observed in a nonreactive solvent such as CCl_4, when HCl is used as the catalyst (*11, 14*). Studies of ether cleavage under the influence of HCl and HBr (*16, 18*) have shown that the protonated ether may react directly or under the influence of a second molecule of HX. When the second HX molecule is present, it provides the nucleophile for attack on the alkyl or benzyl group associated with the ether. In the mechanism shown in Fig. 10, it is assumed that cleavage of the protonated BPE requires a second unit of HCl · $ZnCl_2$. Support for this form of reaction 3 comes from an analysis of the reaction kinetics, as will be discussed. The benzyl chloride formed in step 3 can react further, via step 4, to form benzylxylene.

While it is known that $AlCl_3$ (*11*), $AlBr_3$ (*12*), and BBr_3 (*13*) will catalyze the cleavage of phenolic ethers in the absence of a proton acid, the results presented here suggest that $ZnCl_2$ is too weak a Lewis acid to operate in this fashion. Accordingly, pathways involving $ZnCl_2$ alone have not been incorporated into the mechanism presented in Fig. 10. A pathway involving hydrated $ZnCl_2$ is also not included since water was not found to affect the rate of reaction (Table 2). Consequently, the only form of the catalyst considered to be active is HCl · $ZnCl_2$.

Analysis of the Reaction Kinetics

The reaction mechanism given in Fig. 10 can be used to interpret the reaction kinetics observed in this study. For this purpose the autoclave is modeled as a well-stirred, isothermal, batch reactor. The concentrations of each species present in the reactor can then be expressed by the un-steady-state mass balances given by Eqs. (1)–(7).

$$\frac{dE}{dt} = -k_1ZE + k_{-1}I \tag{1}$$

$$\frac{dZ}{dt} = -k_1ZE + k_4C \tag{2}$$

$$\frac{dI}{dt} = k_1ZE - k_{-1}I - K_2I - k_3ZI \tag{3}$$

$$\frac{dC}{dt} = k_3ZI - k_4C \tag{4}$$

$$\frac{dP}{dt} = k_3ZI \tag{5}$$

$$\frac{dH}{dt} = k_2I \tag{6}$$

$$\frac{dB}{dt} = k_4C \tag{7}$$

where

E = concentration of BPE (M),

Z = concentration of $HCl \cdot ZnCl_2$ times the dispersion of $ZnCl_2$ (M),
I = concentration of protonated ether (M),
P = concentration of phenol (M),
H = concentration of hydroxydiphenylmethane (M),
C = concentration of benzyl chloride (M),
B = concentration of benzylxylene (M).

The species concentrations that appear in these equations are per unit volume of solution and the concentration of catalyst is multiplied by the $ZnCl_2$ dispersion to account for the fact that only the external surface of the $ZnCl_2$ particles is active. The solvent, *p*-xylene, is assumed to be in large excess, and hence, its concentration is taken to be constant.

The initial conditions for Eqs. (1)–(7), at $t = 0$, are given by

$$E = E_0 \qquad H = 0$$
$$Z = Z_0 \qquad P = 0$$
$$I = 0 \qquad P = 0.$$
$$C = 0$$

It is noted that Z_0 represents the initial concentration of $HCl \cdot ZnCl_2$ multiplied by the dispersion of the $ZnCl_2$. Since it is assumed that the HCl added to the $ZnCl_2$ distributes uniformly throughout the catalyst particles, the ratio of HCl to $ZnCl_2$ at the surface of the zinc chloride particles is the same as in the bulk.

The rate coefficients appearing in Eqs. (1)–(7) were determined by fitting the solutions for Eqs. (1) and (4)–(7) to the experimentally observed curves of concentration versus time. The following procedure was used for this purpose. Initial values of the rate coefficients were assumed and the differential equations were integrated using a Runge–Kutta–Gill routine (*25*). The concentration versus time curves obtained from the model were then compared to the experimental curves. If the agreement between theory and experiment was poor, a new set of rate coefficients was chosen and the concentration versus time curves were recalculated. This procedure was repeated until the difference between the predicted and the observed concentration profiles was minimized. A Simplex routine (*26*) was used to select the values of k_1, k_{-1}, k_2, and k_3 that best reproduced the experimental curves. The value for k_4, the rate coefficient for benzyl chloride reaction, was taken from independent experiments and was not adjusted in the course of this procedure.

The solid curves presented in Fig. 1 show the best fit of the concentration versus time profiles to those observed experimentally for the reaction of BPE at 466 K. The values of the rate coefficients used to obtain this fit are given in Table 5. All of the rate coefficients could be defined precisely, since the quality of the fit between the predicted and observed concentration versus time profiles was sensitive to variations in each of the rate parameters.

The participation of $HCl \cdot ZnCl_2$ in step 2 of the mechanism was established by modeling the kinetics of the BPE reaction with and without the participation of $HCl \cdot ZnCl_2$ in this step. In the latter case the term k_3ZI in Eqs. (3)–(5) was replaced by k_3I. Good agreement could be achieved between the predicted and observed concentration versus time profiles using both versions of the model. The rate coefficients for the two cases are given in Table 6. It is apparent that the values of k_1, k_{-1}, and k_2 are virtually the same in both cases and are not strongly dependent on the concentration of HCl. In the case where step 2 is assumed to occur with the participation of $HCl \cdot ZnCl_2$, the value of k_3 is also independent of HCl concentration. However, if it is assumed that step 2 does not involve $HCl \cdot ZnCl_2$, then k_3 increases in proportion to the HCl concentration. This indicates that k_3, in this case, is really a product of the intrinsic rate coefficient and the HCl concentration and, hence, points to the version of step 2 in which $HCl \cdot ZnCl_2$ is present as one of the reaction partners.

TABLE 5

Rate Coefficients

Ether	k_i		466 K	495 K	515 K	k_i^0		E_i (kcal/mol)
BPE	k_1	$\left(\frac{cm^3}{mole \cdot s}\right)$	4.9×10^6	6.5×10^6	13.5×10^6	1.5×10^{11}	$\left(\frac{cm^3}{mole \cdot s}\right)$	9.6
	k_{-1}	(s^{-1})	4.2×10^{-3}	—	—	—		—
	k_2	(s^{-1})	3.7×10^{-3}	4.8×10^{-3}	7.3×10^{-3}	3.7	(s^{-1})	6.4
	k_3	$\left(\frac{cm^3}{mole \cdot s}\right)$	6.2×10^7	2.2×10^8	4.8×10^8	1.4×10^{17}	$\left(\frac{cm^3}{mole \cdot s}\right)$	19.9
BTE	k_1	$\left(\frac{cm^3}{mole \cdot s}\right)$	4.6×10^6	12.3×10^6	3.9×10^7	1.6×10^{16}	$\left(\frac{cm^3}{mole \cdot s}\right)$	20.4
	k_{-1}	(s^{-1})	7.1×10^{-3}	—	—	—		—
	k_2	(s^{-1})	5.6×10^{-3}	7.7×10^{-3}	13.1×10^{-3}	3.1×10^1	(s^{-1})	8.0
	k_3	$\left(\frac{cm^3}{mole \cdot s}\right)$	8.2×10^7	4.4×10^8	10.5×10^8	4.6×10^{19}	$\left(\frac{cm^3}{mole \cdot s}\right)$	25.0
BNE	k_1	$\left(\frac{cm^3}{mole \cdot s}\right)$	3.9×10^6	11.2×10^6	2.3×10^7	4.7×10^{14}	$\left(\frac{cm^3}{mole \cdot s}\right)$	17.2
	k_{-1}	(s^{-1})	3.0×10^{-3}	—	—	—		
	k_2	(s^{-1})	8.6×10^{-3}	1.5×10^{-2}	2.6×10^{-2}	1.3×10^2	(s^{-1})	11.1
	k_3	$\left(\frac{cm^3}{mole \cdot s}\right)$	5.1×10^7	4.0×10^8	8.8×10^8	8.5×10^{20}	$\left(\frac{cm^3}{mole \cdot s}\right)$	28.1

To determine whether the use of a predetermined value of k_4 had any effect on the quality of the fit or the magnitude of the final set of rate coefficients, the fitting procedure was repeated, but this time allowing k_4 to be one of the adjustable parameters.

TABLE 6

Comparison of Rate Coefficients for Models Including and Excluding $HCl \cdot ZnCl_2$ in Reaction 3[a]

	k_i		HCl concn			
			0.007 *M*	0.024 *M*	0.042 *M*	0.120 *M*
Excluding $HCl \cdot ZnCl_2$	k_1	$\left(\frac{cm^3}{mole \cdot s}\right)$	4.2×10^6	5.3×10^6	5.5×10^6	4.2×10^6
	k_{-1}	(s^{-1})	4.7×10^{-3}	4.8×10^{-3}	4.3×10^{-3}	4.5×10^{-3}
	k_2	(s^{-1})	3.3×10^{-3}	2.8×10^{-3}	2.8×10^{-3}	3.0×10^{-3}
	k_3	(s^{-1})	2.5×10^{-3}	7.7×10^{-3}	13.2×10^{-3}	20.2×10^{-3}
Including $HCl \cdot ZnCl_2$	k_1	$\left(\frac{cm^3}{mole \cdot s}\right)$	4.9×10^6	4.5×10^6	5.4×10^6	4.9×10^6
	k_{-1}	(s^{-1})	4.8×10^{-3}	4.2×10^{-3}	4.3×10^{-3}	4.2×10^{-3}
	k_2	(s^{-1})	3.5×10^{-3}	3.7×10^{-3}	3.3×10^{-3}	3.2×10^{-3}
	k_3	$\left(\frac{cm^3}{mole \cdot s}\right)$	5.9×10^7	6.2×10^7	6.1×10^7	5.8×10^7
	k_4	(s^{-1})	4.7×10^{-3} (5.0×10^{-3})[b]	4.7×10^{-3}	3.5×10^{-3}	3.0×10^{-3} (3.1×10^{-3})

[a] All values are for 466 K.

[b] Determined from independent experiments.

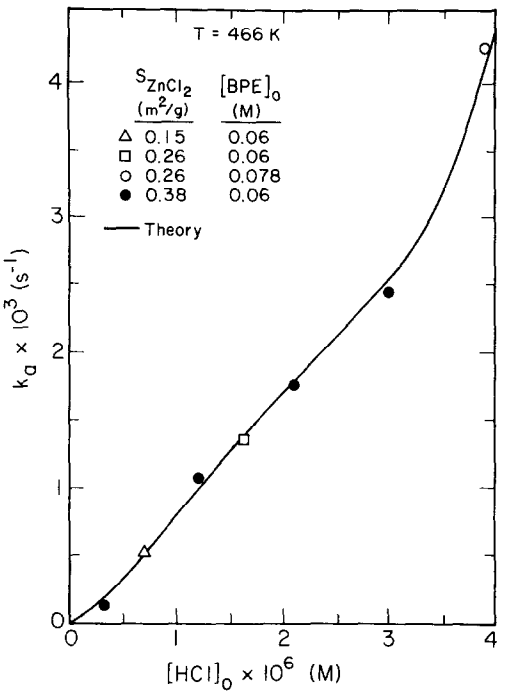

FIG. 11. Effect of the surface concentration of HCl on the apparent rate coefficient for the reaction of BPE.

As may be seen from Table 6, introduction of an additional adjustable parameter has virtually no effect on the values of k_1, k_{-1}, k_2, and k_3 required to obtain an optimal fit. It is also noted that the value of k_4 determined from the fitting procedure agrees very closely with that determined from independent experiments. Repetition of the fitting procedure for several HCl concentrations reveals that the values of k_1, k_{-1}, k_2, and k_3 are nearly independent of HCl concentration. The values of k_4 determined from the fitting procedure continue to be in good agreement with those determined experimentally, and show a slight decrease with increasing HCl concentration. The reason for this is not understood. One possibility is that $ZnCl_2$ is a more active catalyst for the benzyl chloride reaction than HCl · $ZnCl_2$.

The values of k_a determined from the predicted curves of BPE concentration versus time agree very closely with those determined from experimental data. An illustration of this point is shown in Fig. 11. The dependence of k_a on the concentration of HCl at the surface of the $ZnCl_2$ particles predicted by the model is given by the solid curve. The experimental data, represented by the open and closed points, are taken from Figs. 5 and 8. It is quite apparent that the agreement between theory and experiment is very good. Furthermore, Fig. 11 shows that the dependence of k_a on the concentration of HCl in solution and the surface area of the $ZnCl_2$ particles can be represented by a single variable, namely, the concentration of HCl present at the surface of the $ZnCl_2$ particles.

The nonlinear shape of the plot of k_a versus the surface concentration of HCl in Fig. 11 can also be explained. For low to moderate concentrations of HCl, it can be assumed that the concentrations of protonated BPE and benzyl chloride are given by the algebraic equations obtained by invoking the steady-state approximation for Eqs. (3) and (4). The rate of ether disappearance is then

$$\frac{dE}{dt} = \frac{k_1(k_2 + k_3Z)ZE}{k_{-1} + k_2 + k_3Z} = k_aE. \qquad (8)$$

At low values of Z, $(k_{-1} + k_2) > k_3Z$ and $k_a = [k_1k_2/(k_1 + k_2)]Z$. Using the rate coefficients given in Table 5, it is determined that this approximation holds for initial surface HCl concentrations less than 5.0×10^{-7} M. At higher values of Z, $(k_{-1} + k_2) < k_3Z$ and $k_a = k_1Z$. The linear dependence of k_a on Z obtained in this case will hold up to $Z = 3 \times 10^{-6}$ M. Above this level, the steady-state approximations used to obtain Eq. (8) are no longer valid. The apparent rate coefficient is now larger than that predicted by Eq. (8). This behavior is seen in Fig. 11 where it is observed that k_a increases in a faster than linear manner for $Z > 3.6 \times 10^{-6}$ M.

The proposed model, together with the rate coefficients listed in Table 5, also properly predict the effects of changes in initial

concentrations of BPE and *p*-xylene. Thus, for example, it is observed that the value of k_a, determined theoretically, is independent of BPE concentration. The model also predicts the observed fourfold decrease in k_a when the *p*-xylene is diluted to a 50% mole fraction with cyclohexane. This behavior is due to a twofold decrease in the rate at which benzyl chloride reacts, and hence the rate at which $HCl \cdot ZnCl_2$ is regenerated and made available for interaction with BPE.

Comparison of Ethers

The mechanism presented in Fig. 10 can also be used to describe the reaction kinetics for BTE and BNE. By adjusting the rate parameters involved in Eqs. (1) through (7), good agreement was achieved between the experimentally observed, and theoretically predicted, curves of concentration versus time for all components involved in the reactions of both ethers. This point is illustrated in Figs. 2 and 3. The solid curves shown in these plots represent the optimal fit of theory to experiment.

With the exception of k_{-1}, the values of the rate parameters associated with each of the elementary reactions of the mechanism could be determined at different temperatures for all three ethers. A value for k_{-1} could only be determined at 466 K. At higher temperatures, the fits between predicted and observed concentration versus time profiles were found to be insensitive to the magnitude of k_{-1}. It was found that k_{-1} could assume any reasonable value (0–0.1 s^{-1}) without affecting the concentration versus time curves. As a consequence, k_{-1} was usually set to zero for temperatures above 466 K.

Values of the rate coefficients for reactions 1, −1, 2, and 3 are given in Table 3 for BPE, BTE, and BNE. Also given are the preexponential factors, k_i^0, and activation energies, E_i, for reactions 1, 2, and 3. The activation energies follow the same relative order for each ether. Reaction 3, the dissociation of the protonated ether, has the highest activation energy. Reaction 1, the protonation of the ether, has a significantly lower activation energy. Comparison of the three ethers shows that the activation energies for reaction 1 fall in the order BTE > BNE > BPE. The preexponential factors follow an identical sequence. As a result, there is a temperature, 473 K, at which the three ethers have equal values for k_1. Above 473 K, the values for k_1 fall in the same order as the activation energies. This is also the order that was found for k_a and is due to the relative slowness of reaction 1 at higher temperatures. The lower activation energy for reaction 1 versus reaction 3 results in the first reaction becoming relatively slow at higher temperatures. The rate of reaction 1 begins to dominate the reaction rate and the apparent rate coefficient follows the same order for the ethers as does k_1. The dominance of reaction 1 is also the reason for the insensitivity to k_{-1} at higher temperatures. The concentration of protonated ether is roughly proportional to k_1/k_2 and this ratio decreases at higher temperatures. The amount of intermediate and the relative importance of the reverse reaction decreases as the temperature increases.

The activation energies and preexponential factors for the rearrangement of the protonated ether, reaction 2, decrease in the order BNE > BTE > BPE. The magnitude of k_2 follows a similar sequence. This trend is consistent with the relative electron-donating ability of the aryl group and has been observed previously (*11, 23*). The activation energies and preexponential factors for cleavage of the protonated ether, reaction 3, also decrease in the order BNE > BTE > BPE. The trend in the activation energies can be explained as follows. Protonation of the ether oxygen results in a reduction of the electron density of the oxygen. This loss is offset by charge transfer from either the oxygen–methylene bond or the oxygen–aryl bond. As the electron-donating ability of the aryl group increases, more of this electron density comes from the aryl group and the oxygen–methylene

bond becomes stronger. Consistent with this, the activation energy for breaking the oxygen–methylene bond increases with an increase in the electron-donating ability of the aryl group.

Comparison of the experiments using mixed halides provides insight into the respective roles of the hydrogen halide and the zinc halide. It will be recalled that when the initial catalyst is HCl · $ZnBr_2$, the rate of reaction is the same initially as that observed for HCl · $ZnCl_2$. As the reaction proceeds, benzyl bromide is formed and the rate of reaction increases. If, on the other hand, the initial catalyst is HBr · $ZnCl_2$, the initial rate is similar to that observed using HBr · $ZnBr_2$ as the catalyst. In this case, benzyl chloride is produced as the rate of reaction declines. It is apparent from these results that the halide associated with the hydrogen halide is far more significant than the halide associated with the zinc halide. Moreover, in agreement with earlier studies using HX alone (*11*), HBr · ZnX_2 is more active than HCl · ZnX_2. This suggests that the zinc halide is predominantly a carrier for the hydrogen halide. The change in activity of the mixed halide systems can then be attributed to an exchange between the halide of the zinc halide and the hydrogen halide.

The mechanism by which halide exchange occurs between the two components of the catalyst cannot be established definitively from the experiments reported here. At least two possible schemes might be envisioned. The first is direct halide exchange between the hydrogen halide and the zinc halide. The second possibility is that exchange proceeds with the aid of the benzyl halide formed as an intermediate product. The latter type of process is precedented in Friedel–Crafts chemistry (*27*) and is exemplified by the reaction

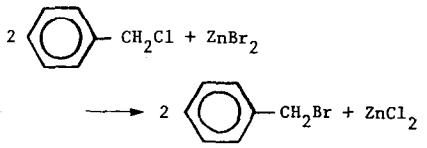

The results presented in Table 3 do show that halide exchange is not limited to the exterior surface of the zinc halide particles. Due to the low surface area of the zinc halides, only 0.03 to 0.08% of the total zinc halide is present at the surface of the particles. On the other hand, more than 2% of the halide associated with the zinc is exchanged during the course of the experiments performed with the mixed halide catalyst systems.

CONCLUSIONS

HCl in combination with $ZnCl_2$ is an active catalyst for the cleavage and rearrangement of benzylaryl ether. While $ZnCl_2$ itself is catalytically inactive, it immobilizes the HCl through the formation of a stable adduct. The results presented here show that HCl penetrates into the interior of small $ZnCl_2$ particles but that it is only the HCl present at the particle exterior which contributes to catalysis. HBr in combination with $ZnBr_2$ behaves in a manner similar to HCl/$ZnCl_2$ but is nearly tenfold more active. When HBr is combined with $ZnCl_2$, the initial catalyst activity is representative of the hydrogen halide. However, with progress of the reaction halide exchange occurs between the hydrogen halide and the zinc halide and the catalyst activity changes.

BPE, BTE, and BNE react in a similar fashion. In each case, cleavage of the ether occurs at the oxygen–methylene bond. Thus, for example, in xylene solution, BPE produces phenol and benzylxylene. A small amount of benzyl halide is also formed as an intermediate product. About 15% of the BPE reacting undergoes rearrangement to form hydroxydiphenylmethane, a product which is stable to further reaction. The extent of cleavage versus rearrangement progresses in the order BPE ~ BTE > BNE. Neither temperature nor H_2 partial pressure influences the product distribution.

The reaction kinetics for BPE, BTE, and BNE can be described in terms of a carbo-

cation mechanism. The first step in the reaction sequence is protonation of the ether oxygen. This adduct then reacts via two parallel pathways. The first results in the rearrangement of the ether to produce the corresponding hydroxydiarylmethane. The second path leads to the formation of benzyl chloride and the aryl alcohol. The benzyl chloride then reacts with the solvent, xylene, to form benzylxylene. The reaction kinetics of all three ethers are accurately described by this mechanism. The rate parameters for individual reaction steps can be determined by fitting the observed product concentration versus time curves to those predicted theoretically. The rate parameters for protonation of the ether and cleavage of the oxygen–methylene bond depend on the ether composition. Both the preexponential factor and the activation energy for the protonation reaction decrease in the order BTE > BNE > BPE. On the other hand, the preexponential factor and activation energy for cleavage of the oxygen–methylene bond decrease in the order BNE > BTE > BPE.

The extent to which HCl · $ZnCl_2$ participates in the cleavage of ether linkages during coal liquefaction in the presence of $ZnCl_2$ is not known. It is of interest to note, though, that McCandless *et al.* (*28*) have observed higher liquid yields when HCl was used in combination with $ZnCl_2$ than when either catalyst was used alone. Since these data were obtained at low coal conversions (<40%), and since ether linkages are one of the first structures to undergo reaction during liquefaction, it is quite likely that the catalyst influenced the rate of ether cleavage. A further point worth noting is that catalysis by HCl · $ZnCl_2$ could occur during the liquefaction of coal, even without the addition of HCl. Evidence for this is given by Zielke *et al.* (*6, 7*), who have observed that HCl is formed during liquefaction in the presence of $ZnCl_2$. The production of HCl is believed to result from the liberation of chlorine when $ZnCl_2$ reacts with sulfur to form ZnS.

ACKNOWLEDGMENTS

This work was supported by the Division of Chemical Sciences, Office of the Basic Energy Sciences, U.S. Department of Energy under Contract DE-AC03-76SF00098.

REFERENCES

1. Whitehurst, D. D. (Ed.), "Coal Liquefaction Fundamentals," ACS Symposium Series 139. Amer. Chem. Soc., Washington, D.C., 1980.
2. Ignasiak, B. S., and Gawlak, M., *Fuel,* **26,** 216 (1977).
3. Roberto, R. G., Cronauer, D. C., Jewell, D. M., and Sehadri, K. S., *Fuel* **56,** 25 (1977).
4. Yao, T., and Kamiya, Y., *Bull. Chem. Soc. Japan* **52,** 201 (1979).
5. Schlosberg, R. H., Davis, W. H., and Ashe, T. R., *Fuel* **60,** 201 (1981).
6. Zielke, C. W., Struck, R. T., Evans, J. M., Costanza, C. P., and Gorin, E., *Ind. Eng. Chem. Proc. Design Dev.* **5,** 158 (1966).
7. Struck, R. T., Clark, W. E., Dudt, P. J., Rosenhoover, W. A., Zielke, C. W., and Gorin, E., *Ind. Eng. Chem. Proc. Design Dev.* **8,** 546 (1969).
8. Wood, R. E., and Wiser, W. H., *Ind. Eng. Chem. Proc. Design Dev.* **15,** 144 (1976).
9. Grens, E. A., Hershkowitz, F., Holten, R. R., Shinn, J. H., and Vermeulen, T., *Ind. Eng. Chem. Proc. Design Dev.* **19,** 396 (1980).
10. Mobley, D. P., and Bell, A. T., *Fuel* **58,** 661 (1979).
11. Palmer, M. H., and McVie, G. J., *J. Chem. Soc. B,* 742 (1968).
12. Tarbell, D. S., and Petropoulos, J. C., *J. Amer. Chem. Soc.* **74,** 244 (1952).
13. McOmie, J. F. W., Watts, M. L., and West, D. E., *Tetrahedron* **24,** 2289 (1968).
14. Schriesheim, A., *in* "Friedel–Crafts and Related Reactions" (G. A. Olah, Ed.), Vol. 4, pp. 477–595. Wiley, New York, 1964.
15. Duffy, J. A., and Ingram, M. D., *Inorg. Chem.* **16,** 2988 (1977).
16. Staude, E., and Patat, F., *in* "The Chemistry of the Ether Linkage" (S. Patai, Ed.), p. 23. Wiley, New York, 1967.
17. Oelschlager, H., Linde, H., Gotze, G., and Iglesias-Meier, J., *Arch. Pharmacol.* **313,** 897 (1980).
18. Okamoto, K., Takeuchi, K., and Shingu, H., *Bull. Chem. Soc. Japan* **37,** 276 (1964).
19. Hart, H., and Elia, R. J., *J. Amer. Chem. Soc.* **83,** 985 (1961).
20. Drummond, A. Y., and Eastham, A. M., *J. Amer. Chem. Soc.* **79,** 3689 (1957).
21. Christian, S. D., and Kennen, B. M., *J. Phys. Chem.* **78,** 432 (1974).

22. Burdham, R. A., Ludman, C. J., Lynch, R. J., and Waddington, T. C., *J. Magn. Reson.* **34,** 223 (1979).
23. Shine, H. J., *in* "Reaction Mechanisms in Organic Chemistry" (C. Eaborn and N. B. Chapman, Eds.), pp. 82–121. Elsevier, New York, 1967.
24. Taylor, N. D., and Bell, A. T., *Fuel* **59,** 499 (1980).
25. Lapidus, L., "Digital Computation," p. 89. McGraw–Hill, New York, 1962.
26. Beveridge, G. S., and Schechter, R. S., "Optimization: Theory and Practice," p. 367. McGraw–Hill, New York, 1970.
27. Drahowzal, F. A., *in* "Friedel–Crafts and Related Reactions" (G. A. Olah, Ed.), Vol. 2, Part 1, pp. 417–475. Wiley, New York, 1964.
28. McCandless, F. P., Waterman, J. J., and Sire, D. S., *Ind. Eng. Chem. Proc. Design Dev.* **20,** 91 (1981).